## 21.7 An Integrated Gravimetric FBAR Circuit for Operation in Liquids Using a Flip-Chip Extended 0.13µm CMOS Technology

M. Augustyniak[1,5], W. Weber[2], G. Beer[2], H. Mulatz[1], L. Elbrecht[2], H.-J. Timme[2], M. Tiebout[2], W. Simbürger[2], C. Paulus[3], B. Eversmann[3], D. Schmitt-Landsiedel[1], R. Thewes[4], R. Brederlow[5]

[1]TU Munich, Munich, Germany, [2]Infineon Technologies, Munich, Germany
[3]Siemens, Munich, Germany, [4]Qimonda, Munich, Germany,
[5]now with Texas Instruments, Freising, Germany

We present a gravimetric sensor based on a film bulk acoustic wave resonator (FBAR) [1-8]. FBAR technology offers thin-film piezoelectric resonators whose frequencies (1 to 2GHz) are much higher than common piezoelectric elements like quartz due to reduced thickness of the piezoelectric layer. Since the electrical properties of FBARs depend on the acoustic impedance of the surrounding medium (air, liquid) and on the mass attached to the surface, a wide range of sensor applications appears feasible. Its high resonant frequency results in high sensitivity for FBAR-based oscillators to changes in surface mass properties [5,6]. A general purpose approach to such gravimetric sensor concepts, with special emphasis on the oscillator circuitry capable to operate under different environmental conditions (air, liquid), is discussed in this paper.

A cross-section of the technology together with the flip-chip bonded CMOS circuit is shown in Fig. 21.7.1. The FBAR consists of a piezoelectric AlN layer sandwiched between two metal electrodes [1]. The resonant frequency of the resonator is determined by the thickness of the piezoelectric layer and by the mass of the electrodes. To prevent acoustic energy leaking into the substrate, an acoustic mirror (similar to an optical Bragg reflector) is formed by alternating low and high acoustic impedances (W, $SiO_2$) within the substrate. Any solid or liquid film attached to the surface of the sensor leads to a mass - and for liquids also a viscosity – increase at the sensor's surface. This results in a decrease of the FBARs resonant frequency. Furthermore, increasing viscosity at the surface of the top layer decreases the quality factor of the resonator. In a simple approximation (for details see [1,6]) the relative change of the oscillation frequency is proportional to the relative change of the total vibrating mass of the sensor.

Since FBARs operate in the GHz range it is important to have short distances between the sensor and amplifying circuit to minimize parasitic inductance [6]. Therefore, the CMOS-based oscillator is placed as close as possible to the sensor surface via flip-chip bonding (see Fig. 21.7.1 and Fig. 21.7.6).

Before starting the design, S-parameters are measured in air and water to extract an electrical model of the FBAR. The main challenge in the design of a suitable oscillator is the reduction of the quality factor in water [6]. Most circuits used for piezo-oscillators [7-9] are not applicable here since they rely on high quality factors. Figure 21.7.2 presents the oscillator topology used in this paper: The FBAR–capacitor (C0) voltage divider together with the amplifier are intended to satisfy the Barkhausen criterion for oscillation.

Figure 21.7.3 presents the transfer function of the FBAR–C0 voltage divider $Vi/Vo$ when the FBAR is operated in water. C0 has a value of 2.8pF, which is chosen as a compromise between high phase change at resonance (C0↑) and high gain peak (C0 ↓). The phase shift is 30° and the gain peak is -2dB at resonance. The remaining 330° and 5dB (to overcompensate the losses) must be provided by the amplifier. This gain–phase relationship at resonance has to be precisely controlled for all process/temperature corners. Therefore, a Gm-C filter topology is used, which is tunable by changing the transconductor bias current. The amplifier consists of 3 transconductors (Gm1, Gm2, Gm3), 2 capacitors (C1, C2), and a buffer to drive the output voltage *Vo* (Fig. 21.7.2). The amplifier's transfer function is:

$$\frac{Vo}{Vi} = -\frac{Gm1}{Gm2}\frac{1}{\left(1+\frac{sC1}{Gm2}\right)\frac{sC2}{Gm3}}$$

A 330° phase shift between *Vo* and *Vi* is achieved by summing up the following contributions: 180° inversion from the transconductors, 90° from $Gm3/sC2$, and 60° from $1+ sC1/Gm2$, when *Gm2* is negative. The gain-phase relationship (330° at 5dB) is independent of the process, because it is based on the matching of Gm1, Gm2, and Gm3, and C1 and C2.

Figure 21.7.4 shows the circuit implementation of the oscillator. M1 together with current mirror M2/M3 realizes the positive Gm1 in Fig. 21.7.2, M4 realizes Gm2, and M6 Gm3. C1 in Fig. 21.7.2 is the gate-channel capacitance of transistors M4-M6, and C2 is the gate-channel capacitance of M7. M8 is a source follower realizing the output buffer. Capacitance C3 is for DC-decoupling. Transistor groups M2, M3 as well as M1 and M4-M7 are matched in order to guarantee the proper gain-phase relationship. As in every high frequency design, care has been taken to minimize the impact of parasitic impedances (especially wiring capacitances). However, the most important parasitic element is the wire inductance between the sensor and the transistors in the oscillation loop [6]. The chosen packaging allows us to keep the wire length below 600µm (Fig. 21.7.7).

The loop containing M8, I3, R1, M1, M2, M3, M4, I1, M6 and I2 is responsible for biasing all of the transistors in the circuit. Assuming similar gate lengths for M3 and M2, as well as for M6 and M4, the matched currents I1 and I2 determine currents in M1, M2, M3, M4, M6 and in that way control Gm1, Gm2, and Gm3. They are adjustable to compensate for Gm-C variations due to process and temperature fluctuations. For stability, the time constant R1*Cin (Cin = gate capacitance of M1) has to be higher than any other time constant in the loop. I1 is used to assure equal saturation for M1, M4, and M6 for good tracking of Gm1, Gm2 and Gm3 at different bias current levels.

The amplitude of $V_o$ is typically on the order of 100 to 200mV, but can decrease to 20mV in fluids. The comparator in Fig. 21.7.4 is used to generate a digital signal out of $V_o$. When the GATE signal is high, pulses at the output of the amplifier are counted by a 34b counter. Next, when READOUT is high, the counter is configured as a shift register and its state is serially brought to the digital output of the chip. This output provides a measure for the oscillation frequency.

A 0.13µm CMOS test chip was fabricated with 8 resonator-amplifiers (see Fig. 21.7.7). The 8 sites operate sequentially to avoid interference and cross-talk related artifacts. The chip area is 4.4mm², and the area of each oscillator is 0.04mm². On the one hand, this ratio demonstrates the potential for arranging sensor stripes and arrays for multiple sensor applications. On the other hand, a lot of area is presently consumed by on-chip MIM decoupling capacitors. The total current drawn by one active oscillator is 27mA from a 1.7V supply and the static current (mainly biasing of the analog circuits) is 12mA. The measured circuit oscillation frequency in air, 1.861GHz, is close to the resonant frequency extracted from sensor S-parameter measurements, 1.883GHz (cf. Fig. 21.7.6).

Measurements were performed using a pattern generator to control the state of the oscillators and counter, and a logic analyzer for readout of the counter data. The set-up for measurements in fluids is shown in Fig. 21.7.5. S-parameters were measured with open and short structures for de-embedding, and jitter was measured by taking the standard deviation of several counter cycles. The calculated frequency shifts on this basis are shown in Fig. 21.7.6. The measured frequency shifts were 5MHz in ethanol and 7.3MHz in water. The circuit is fully functional with a jitter of less than 3kHz for all operating conditions.

Temperature and mismatch effects can be compensated by performing reference measurements or by using differential principles. Therefore the resolution is mostly limited by jitter. Since the measured jitter is found to be independent of the sensor's quality factor (cf. Fig. 21.7.6: measurements in air and in water), we conclude that the entire resulting inaccuracy is dominated by the jitter of the pattern generator, which triggers and stops the counter in Fig. 21.7.4. With the given setup, even in fluids we achieve a frequency resolution of better than $5\times10^5$ relative to the resonant frequency. This corresponds to a calculated measurement accuracy for surface mass changes in the pg range for a 200×200µm² sensor. For measurement of ethanol concentration in water this corresponds to a resolution of better than 0.2%.

*References:*

[1] R. Aigner et al., "Advancement of MEMs into RF-Filter Applications," *IEDM Tech. Dig.*, pp. 897-900, 2002.
[2] G. Sauerbrey, "Massenwaegung mit Piezoelektrischen Resonatoren," *Zeitschrift für Physik*, Vol. 155, p. 206-217, 1959.
[3] R.V. Bucur, J.-O. Carlsson and V.M. Mecea, "Quartz-Crystal Mass Sensors with Glued Foil Electrodes," *Sensors & Actuators B: Chemical*, pp. 91-95, Nov, 1996.
[4] Y. Li et al., "Very High Q-Factor in Water Achieved by Monolithic, Resonant Cantilever Sensor with Fully Integrated Feedback," *Proc. IEEE Sensors*, vol. 2, p. 809 - 813, 2003.
[5] R. Gabl et al., "Novel Integrated FBAR Sensors: A Universal Technology Platform for Bio- and Gas-detection," *Proc. IEEE Sensors*, vol. 2, p. 1184-1188, 2003.
[6] R. Brederlow et. al., 'Biochemical Sensors Based on Bulk Acoustic Wave Resonators," *IEDM Tech. Dig.*, p. 992-994, 2003.
[7] M.-A. Dubois et al., "Integration of High-Q BAW Resonators and Filters above IC," *ISSCC Dig. Tech. Papers*, pp. 392-393, 2005.
[8] B. Otis, Y.H. Chee and J. Rabaey, "A 400µW-RX, 1.6mW-TX Super-Regenerative Transceiver for Wireless Sensor Networks," *ISSCC Dig. Tech. Papers*, pp. 396-397, 2005.
[9] U. Tietze, C. Schenk, Berlin, Springer, 1993.

 

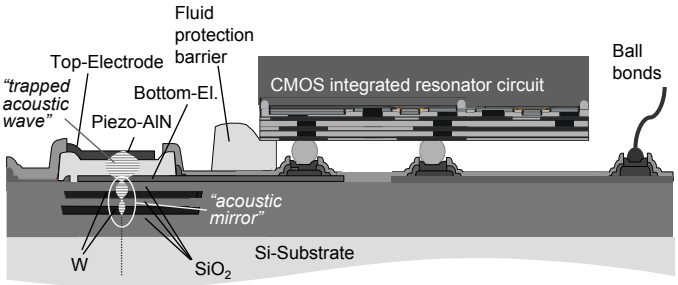


Figure 21.7.1: Schematic representation of the sensor system.

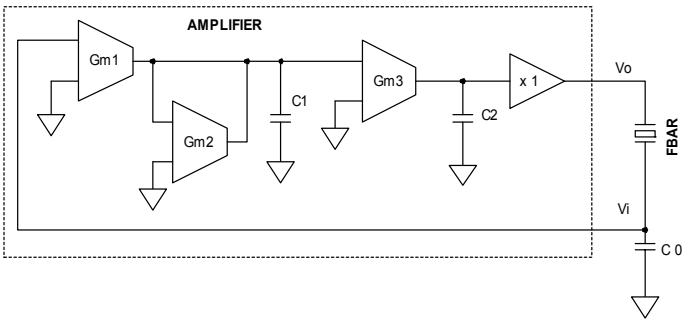


Figure 21.7.2: Oscillator containing FBAR resonator and Gm-C amplifier.

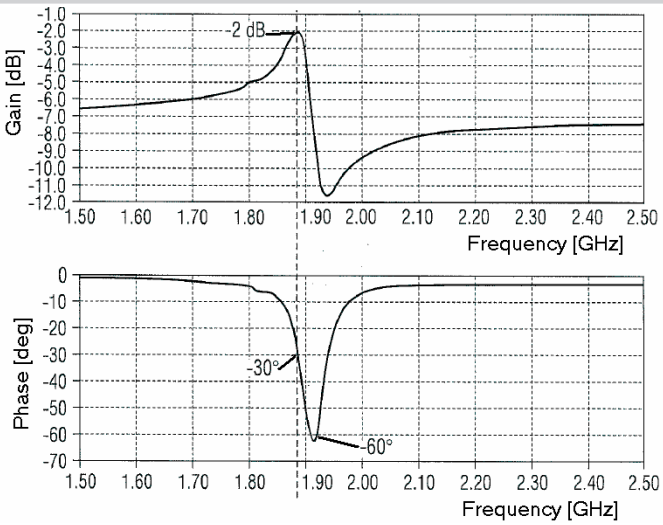


Figure 21.7.3: Gain and phase of FBAR-CO transfer function: *Vi/Vo* versus frequency. The plot shows simulated data based on the model for an FBAR immersed in water. The resonantfrequency is 1.87GHz.

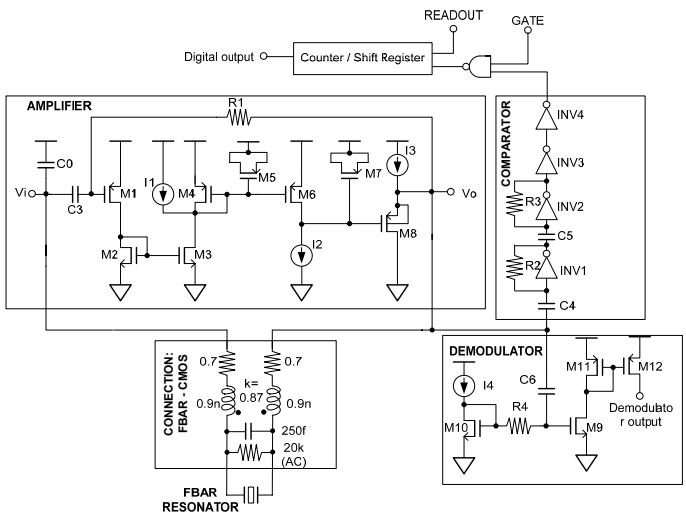


Figure 21.7.4: Implementation of the oscillator circuit.



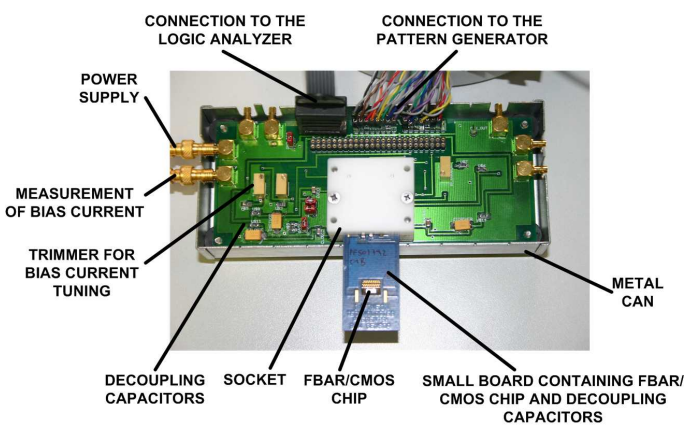


Figure 21.7.5: PCB and measurement set-up suitable for measurements in a liquid environment.

| | | | |
|---|---|---|---|
| CMOS technology used | | | 0.13µm |
| total chip area | | | 4.4mm$^2$ |
| pixel circuit area | | | 0.04mm$^2$ |
| static current | | | 12mA ± 1mA |
| dynamic current per sensor site | | | 16mA ± 1mA |
| oscillation in | air | measured frequency with CMOS circuit operating | 1.861GHz ± 3kHz |
| | | calculated frequency on the basis of measured sensor S-parameters | 1.883GHz |
| | | sensor quality factor | 500 |
| | water | measured frequency shift with CMOS circuit operating | 7.3MHz ± 3kHz |
| | | calculated frequency shift on the basis of measured sensor S-parameters | 6.0MHz |
| | | sensor quality factor | 50 |
| | ethanol | measured frequency shift with CMOS circuit operating | 5.0MHz ± 3kHz |
| | | calculated frequency shift on the basis of measured sensor S-parameters | --- |
| | | sensor quality factor | --- |

Figure 21.7.6: Performance overview of the gravimetric FBAR circuit.

*Continued on Page 610*

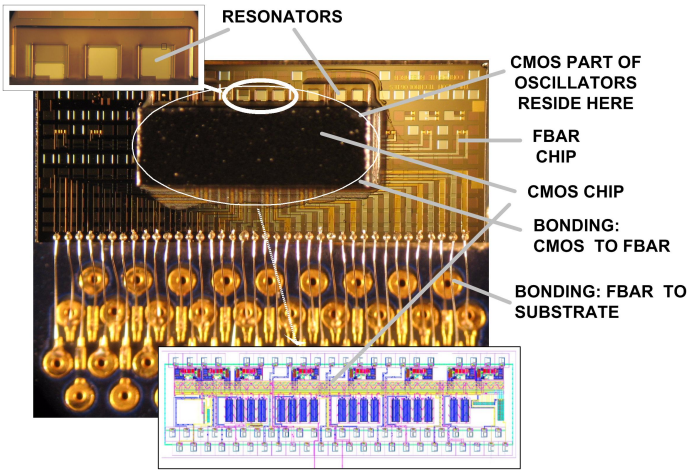


Figure 21.7.7: Chip photo including the bonded area and the flip-chip package.

 